# Ice-rafted dropstones at midlatitudes in the Cretaceous of continental Iberia

Juan Pedro Rodríguez-López[1,2], Carlos L. Liesa[3,*], Aránzazu Luzón[3], Arsenio Muñoz[3,†], María J. Mayayo[3], Julian B. Murton[2], and Ana R. Soria[3]

[1]Department of Geology, Faculty of Science and Technology, University of the Basque Country (UPV/EHU), Apartado 644, E-48080 Bilbao, Spain

[2]Permafrost Laboratory, Department of Geography, University of Sussex, Brighton BN1 9QJ, UK

[3]Departamento de Ciencias de la Tierra–Instituto de Ciencias Ambientales (IUCA), Facultad de Ciencias, Universidad de Zaragoza, Pedro Cerbuna 12, E-50009 Zaragoza, Spain

## ABSTRACT

The Cretaceous is widely considered to have been a period subjected to super-greenhouse conditions. Here, we provide multiscale sedimentologic evidence of glaciers developing at mid-paleolatitudes ($\sim$45°N) in continental Iberia during the Hauterivian cold snap. Striated and faceted ice-rafted glacial dropstones (cobble to boulder size) and striated and grooved silt- to sand-sized grains (ice-rafted debris [IRD]) occur in a lacustrine sequence of the Enciso Group in the eastern Cameros Basin, Spain. The ice-rafted materials constitute the first evidence reported for a Cretaceous continental cryospheric record in Europe, and they are attributed to calving of glacier snouts, releasing icebergs into an ice-contact lake. The sedimentary succession resembles glacial-deglacial records in lakes overridden by the late Pleistocene Laurentide Ice Sheet in eastern Arctic Canada. The Iberian glacial succession was coeval with plateau permafrost in Asia and IRD records in the Arctic and Australia, revealing a stronger than previously thought cryosphere during the global Hauterivian cold snap.

## INTRODUCTION

The widespread view of the Cretaceous Period as an archetypal super-greenhouse is being increasingly questioned by new data (Ladant and Donnadieu, 2016) suggesting that the Cretaceous cryosphere had similarities with its Pleistocene and Holocene counterparts (Rodríguez-López et al., 2022). Evidence of an active cryosphere during the Cretaceous includes glacial dropstones and ice-rafted debris (IRD) transported by icebergs both in marine deposits (Rodríguez-López et al., 2016; Alley et al., 2020) and continental plateau oases (Wu and Rodríguez-López, 2021), and high-altitude permafrost (Rodríguez-López et al., 2022). Such evidence for deep-time glacial and permafrost records is vital for understanding cryosphere

dynamics on very long time scales ($10^6$–$10^8$ yr; Le Heron et al., 2022). Interestingly, Early Cretaceous glaciated seas and continents were coeval with warm oceans and seas (e.g., Littler et al., 2011; Price et al., 2020), revealing a more complex climate system than previously supposed.

Here, we report the occurrence of glacial dropstones and IRD in lacustrine deposits from the Lower Cretaceous section in the Cameros Basin, Spain, attributed to a deglaciation sequence that demonstrates an active cryosphere at unexpected mid-paleolatitudes during the archetypal Cretaceous super-greenhouse.

## GEOLOGIC BACKGROUND AND STUDY AREA

The Cameros Basin is a continental rift basin (30–70 km wide, 150 km long) that was located at midlatitudes (42°N–50°N) during the Early Cretaceous and developed within the Iberian microplate during the opening of the western

Tethys and the North Atlantic Oceans (Nirrengarten et al., 2017; King et al., 2021). The basin contains a mostly continental synrift succession ($\sim$8 km thick, Tithonian–Albian). Here, we report ice-rafted dropstones and IRD from the Enciso Group (Hauterivian–early Barremian; Muñoz et al., 2020) in Navalsaz, northern Spain (Fig. 1B; Fig. S1A in the Supplemental Material[1]), where this group is $\sim$1.4 km thick and consists of carbonate and siliciclastic lacustrine deposits (Figs. S1A–S1B and S2).

## ICE-RAFTED MATERIAL

Cobble- and boulder-sized dropstones (Figs. 1C–1I and 2A–2B; Figs. S2–S5) and silt- to sand-sized IRD (Figs. 2B and 3A–3G; Fig. S7) were observed in three different glacial lithofacies (Figs. 2A, 2B, and 2E): (1) restricted glaciolacustrine black shales (Figs. 2A–2B and 3F–3G); (2) laminated glaciolacustrine silts (Figs. 2A–2B and 3A–3E; Figs. S7D–S7E); and (3) proglacial subglacial sandy lobes related to glacier front retreat (Figs. 2A–2B; Figs. S7A–S7C).

### Cobble- and Boulder-Sized Dropstones

A 1.4-m-thick succession of the Enciso Group revealed ice-rafted glacial dropstones both at outcrop (Figs. 1C–1I and 2A–2B; Figs. S2–S5) and at microscopic scales (IRD) (Figs. 2B and 3F–3G; Fig. S7) (see Supplemental Material text, figures, and table). Across an $\sim$20-m-long outcrop, 22 dropstones were observed, at different stratigraphic levels, in a 0.5-m-thick sedimentary interval formed by parallel-stratified silty glaciolacustrine litho-

Carlos L. Liesa ⓘ https://orcid.org/0000-0002-9130-117X
*carluis@unizar.es
†deceased

CITATION: Rodríguez-López, J.P., et al., 2023, Ice-rafted dropstones at midlatitudes in the Cretaceous of continental Iberia: Geology, v. XX, p. , https://doi.org/10.1130/G51725.1
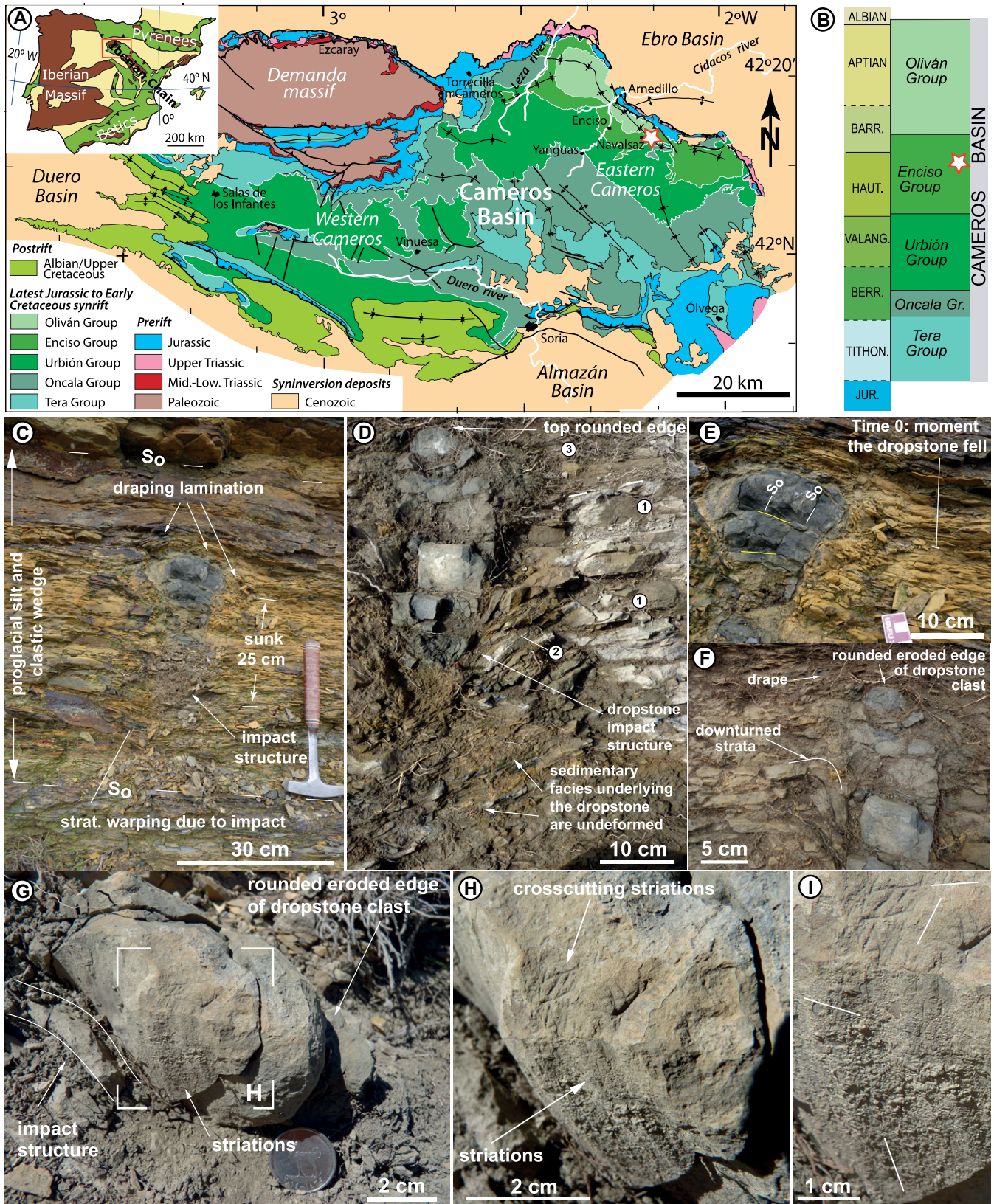
Figure 1. (A) Geologic map of Cameros Basin and location of studied area (star). (B) Chronostratigraphic and lithostratigraphic units showing location of glacial dropstones (star). Barr—Barremian; Haut—Hauterivian; Valang—Valanginian; Berr—Berriasian; Tithon—Tithonian; Jur—Jurassic. (C) Glacial dropstone impacted in horizontally bedded siltstones ($S_0$—depositional stratification planes; see Fig. S3 [text footnote 1]). (D) Dropstone with rounded edges and long axis perpendicular to bedding encased in ocher laminated siltstones (see Figs. S4 and S5 [text footnote 1]); (1) horizontal siltstones, (2) downturned lamination due to impact, and (3) siltstones draping and onlapping rounded dropstone top. (E) Detail of C, showing dropstone lamination and inherited fractures. (F) Detail of D showing downturned strata due to dropstone impact and the draping of the rounded dropstone top by overlying siltstones. (G) Dropstone with rounded edge and facets with striations. Warped stratification is due to dropstone impact. (H) Close-up view of G, showing striations. (I) Close-up view of H.
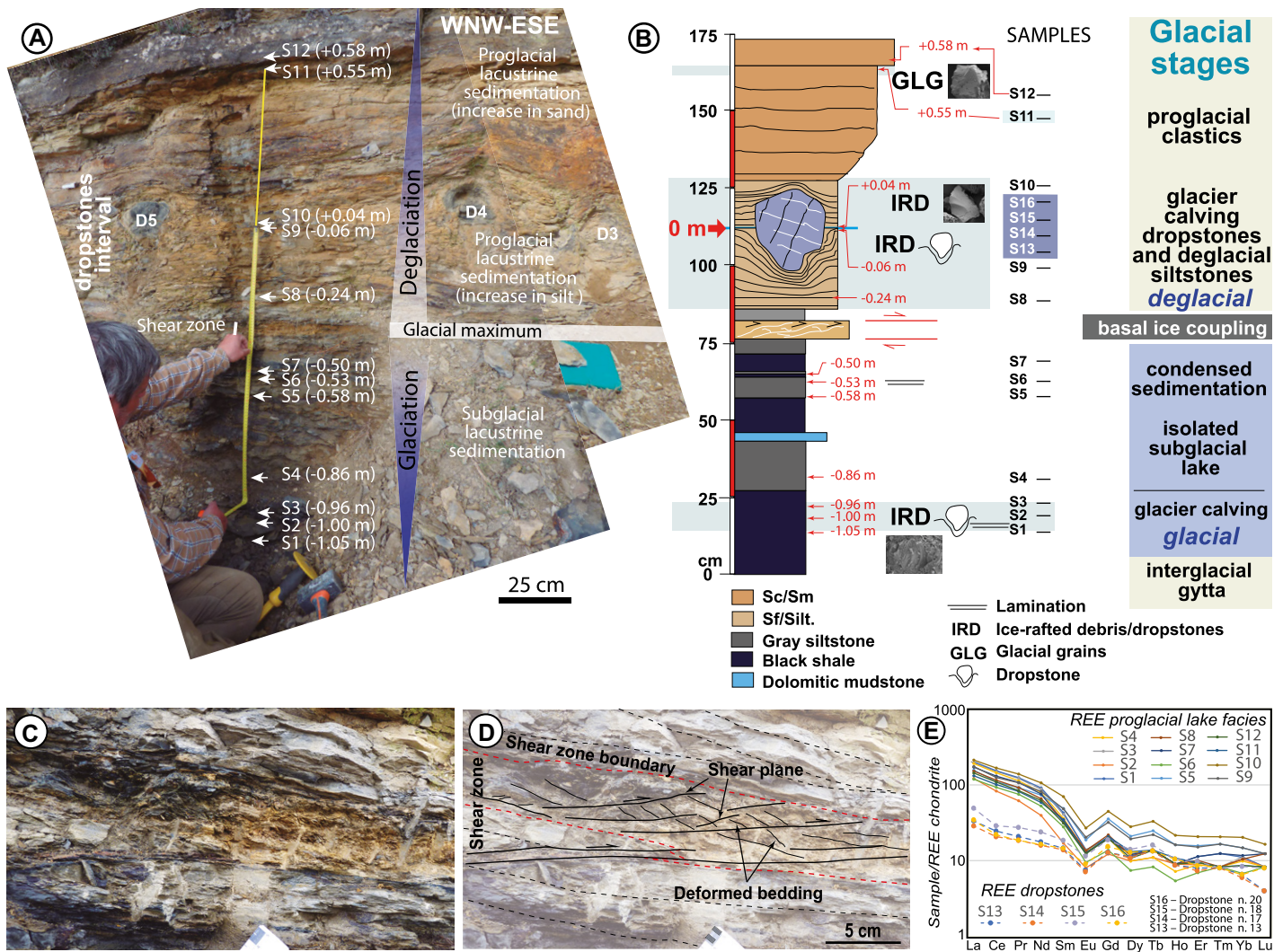
Figure 2. (A) Outcrop of facies deposited during glacial-deglacial cycle. Locations of samples (S1 to S12, with their stratigraphic position in m) and three dropstones (D3, D4, and D5) are shown. (B) Glacial-deglacial succession showing lithofacies, position of ice-rafted debris (IRD), and glacial stages. (C) Field photograph and (D) line drawing of basal ice–related shear band at ∼0.75 m. (E) Rare earth element (REE) geochemistry of proglacial lacustrine lithofacies and glacial dropstones (values normalized to chondrite; Anders and Grevesse, 1989). Sc/Sm—coarse/medium-grained sandstone; Sf/Silt.—fine-grained sandstone/siltstone.

facies (Figs. 2A–2B; Figs. S1–S5). The dropstones occur as dispersed, outsized cobble to boulder limestone clasts, with polished, faceted surfaces (Figs. 1C–1F; Fig. S3) and crosscutting striations (Figs. 1G–1I). They generated impact structures in the sediment beneath (Figs. 1C–1F; Figs. S3–S5), including downturning of the host stratification by up to 90° (Figs. 1D and 1F; Figs. S4D and S5A–S5D), observable at the dropstone margins, and truncation of stratification and lamination (Figs. 1D–1F; Figs. S4A–S4F). Undisturbed laminated shales and siltstones above the dropstones represent subsequent draping lamination (Figs. 1C–1F; Figs. S3A–S3E and S4G).

Geochemical signatures of the dropstones differ from the host laminated lithofacies (Fig. 2E; Fig. S2A). The dropstones display the original bedding ($S_0$) and inherited millimeter-thick tension veins, which are rotated and unconformable with respect to the host lithofacies lamination (Fig. 1E). Fifty percent of the

outsized clasts have their long axes perpendicular to the bedding plane (Figs. 1C–1F; Figs. S3–S6). Morphometric analysis indicated dropstone penetration depths up to 30 cm and bending of underlying bedding by up to 20 cm beneath the base of the dropstones (Supplemental Material text; Table S1; Fig. S6). Collectively, these features are attributed to ice-rafted dropstones released from lacustrine icebergs and emplaced on the lake bottom (Le Heron, 2015; Le Heron et al., 2021; Rodríguez-López et al., 2016; Wu and Rodríguez-López, 2021). The quantified penetration depths and bending of underlying strata suggest that glacial dropstones were released into a relatively deep lake.

**Silt- to Sand-Sized IRD**

The lithofacies hosting the outsized glacial dropstones also contain silt- to sand-sized IRD (Figs. 2B and 3; Fig. S7), which appears as dispersed, angular quartz clasts (>60 μm). The sur-

faces of these grains show striations (Figs. 3B, 3C, and 3E), conchoidal fractures (Figs. 3A–3D; Figs. S7A–S7D), and trails of crescentic gouges in association with curved grooves (Figs. 3B–3C and 3E).

The stratigraphic interval containing the dropstones and IRD rests on a 0.8-m-thick unde-formed bed of parallel-stratified black shales and dark-gray mudstones that also contain dispersed IRD (>200 μm in size; Figs. 2B and 3F–3G). These IRD grains also display surfaces with striations and conchoidal fractures (Figs. 3F–3G) and are scattered in the laminated black shales, draped by onlapping lamination (Fig. 3F). The top of this lower level shows a 5–10-cm-thick shear zone horizon (at 0.75 m) covered by unde-formed black shales (Figs. 2A–2B).

The distribution of IRD along the studied interval, geometric relationships with host sediments, and the surficial characteristics of IRD, including conchoidal fractures and striations, are consistent with transport in a subglacial environ-
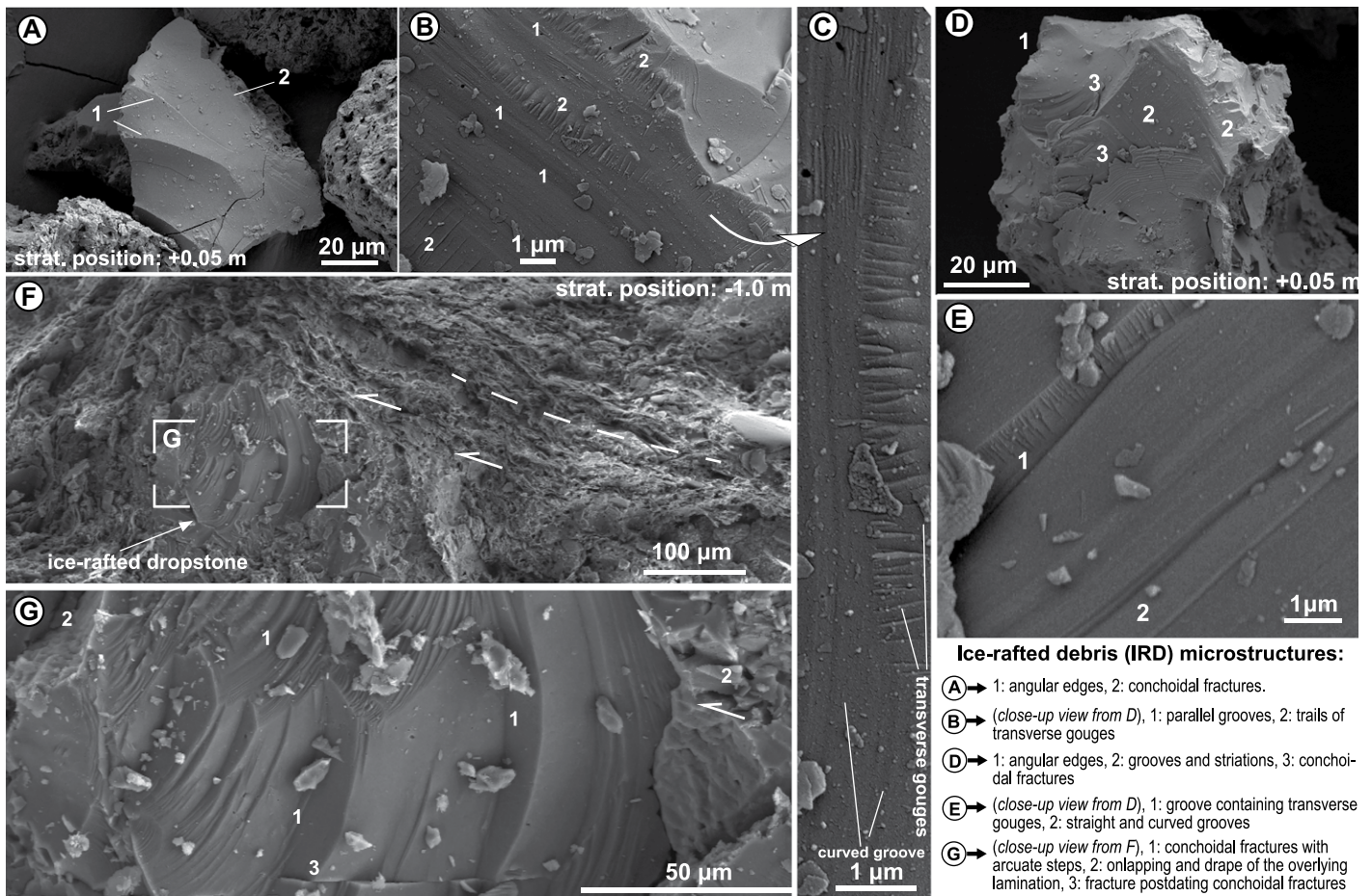
**Figure 3.** Field emission scanning electron microscope (FESEM) images of ice-rafted debris (IRD): (A) IRD (position +0.05 m, Fig. 2B), with angular edges (1) and conchoidal fractures (2). (B) Close-up view of D, showing parallel grooves and trails of transverse and lunate gouges. (C) Detail of B showing curved grooves, striations, and transverse straight and lunate gouges. (D) IRD (position +0.05 m, Fig. 2B), showing angular edges (1), grooves and striations (2), and conchoidal fractures (3). (E) Close-up view of D, showing groove with transverse gouges (1) and straight and curved grooves (2). (F) Sand-sized dropstone with conchoidal structures encased in black shales (position −1.0 m, Fig. 2B). Arrows indicate drape of lamination covering dropstone protrusion. (G) Detail of F, showing conchoidal fractures (1) with arcuate steps, onlapping and drape of overlying lamination (2), and fracture (3) postdating conchoidal fractures.

ment (Le Heron et al., 2020), with fracturing and mechanical crushing by rock fragments, and their release to the lake from glacier calving (Xia et al., 2023). Glacially crushed quartz grains (Figs. 3A and 3D) with transverse crescentic fractures along the strike associated with striations (Figs. 3B–3C) are similar to those attributed to ice-sheet action from the Pliocene of Canada (Gao et al., 2012). Such grains likely formed in a subglacial environment characterized by fracturing and mechanical grinding under the glacial overburden pressure (e.g., Gao et al., 2012; Le Heron et al., 2020). Troughs with flat floors containing trails of transverse gouges associated with deep grooves and striations (Fig. 3E; Fig. S7E) also formed during subglacial transport (cf. Gao et al., 2012). Angular and subangular quartz grains with ubiquitous, large conchoidal fractures and associated grooves (Fig. 3; Figs. S7A–S7D) have been observed in glacial sediments of Russell Glacier, Greenland (Kalińska-Nartiša et al., 2017). Similar angular grains with grooves and striations (Figs. 3D–3E) have been

reported from recent glacial diamicts from East Antarctica (Shrivastava et al., 2014), from Proterozoic glacial diamictites in Brazil (Araújo and Nogueira, 2019), and from the Lower Cretaceous section of Australia (Alley et al., 2020).

Angular quartz grains with striations, grooves, and conchoidal fractures (Fig. 3; Fig. S7) attributed to subglacial transport (e.g., Le Heron et al., 2020) also occur in the 0.5-m-thick clastic wedge (subglacial fan) that overlies the interval containing the boulder-sized glacial dropstones and IRD (Figs. 2A–2B; Fig. S7A), which were incorporated into the prograding deglacial clastic wedge when subglacial meltwaters reached the proglacial lake.

## DISCUSSION AND CONCLUSIONS
### Cretaceous Glacial-Deglacial Cycle and Its Pleistocene Analogue

The Cretaceous succession from Iberia resembles lacustrine sediment sequences related to Pleistocene glacial-deglacial cycles of the Laurentide Ice Sheet (LIS) in the eastern Cana-

dian Arctic (fig. 3 of Briner et al., 2007). Four stages are differentiated (Fig. 4A): (1) deposition of the lowermost black shales predating the glacial-deglacial succession (Figs. 2A–2B); (2) glacial advance across the lake (2 in Fig. 4A), where calving and melting of icebergs and growlers released IRD (0–25 cm interval; Figs. 2B and 3F–3G), and geochemical anomalies (Fig. S2) are associated with meltwater plumes entering the lake (cf. Stevenard et al., 2022); (3) further advance of the glacier, progressive subglacial lake isolation, condensation and accumulation of black shales with IRD (25–75 cm interval in Figs. 2A–2B; see also fig. 3C of Briner et al., 2007), and geochemical anomalies (e.g., Na, U, Ag; samples S5, S6, and S7 in Fig. S2); and (4) onset of deglaciation, with dropstones and IRD deposition from melting icebergs due to frequent calving of the ice front. The maximum glacial advance (stage 3) led to coupling of the basal glacier ice with the lake-bottom sediments, triggering shear deformation (Figs. 2B–2D, at 0.75 m), with overlying undeformed black
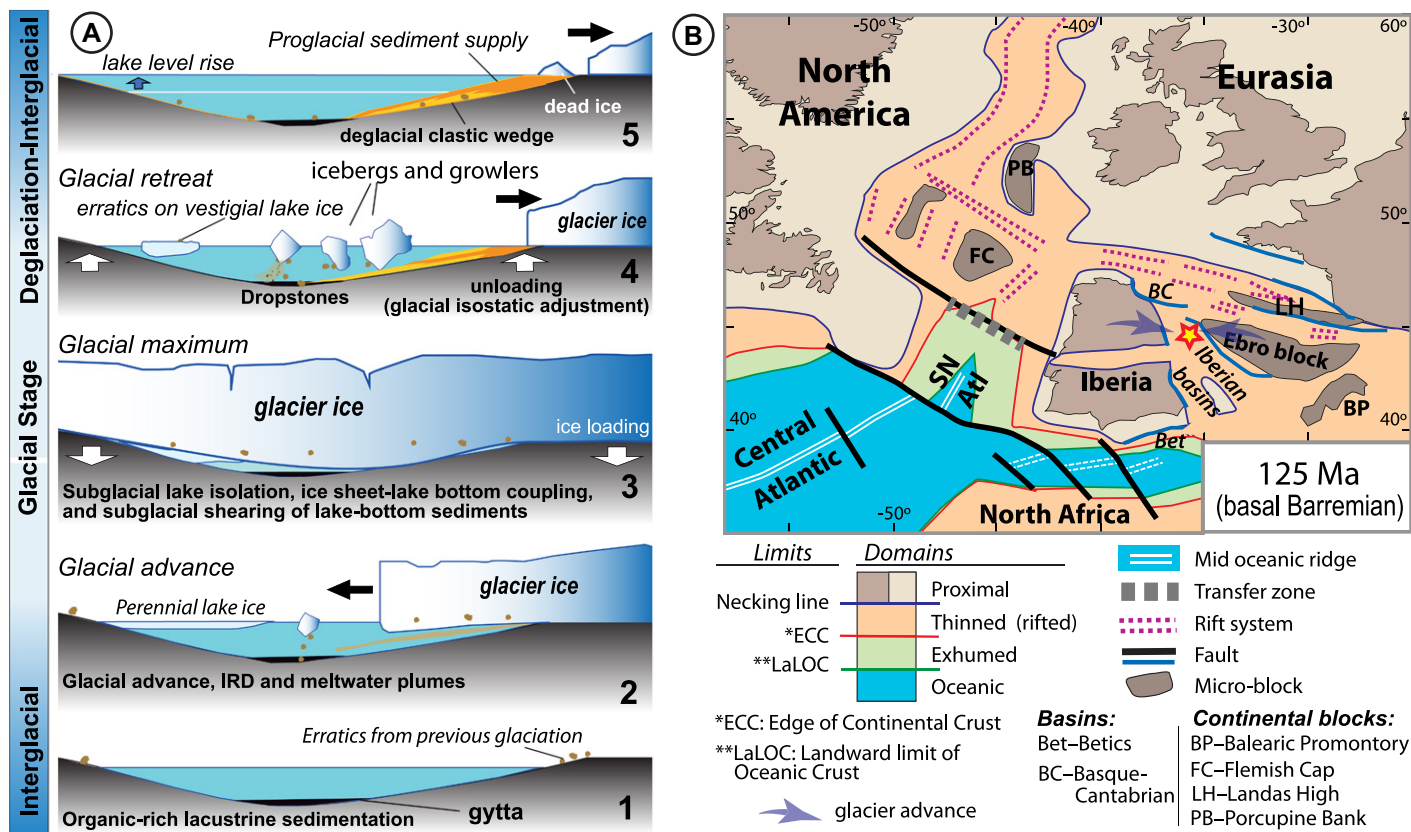
**Figure 4.** (A) Evolutionary model of Cretaceous glacial-deglacial cycle in proglacial lake–glacier terminus in Iberia (modified from Briner et al., 2007). (B) Paleoenvironmental restoration of southern North Atlantic (SN Atl), with North America fixed on present-day coordinates, and rifted domains (based on Nirrengarten et al., 2017; Angrand and Mouthereau, 2021; Asti et al., 2022). Star shows location of Cameros Basin. IRD—ice-rafted debris.

shales attesting to resumed subglacial sedimentation and basal ice–sediment decoupling. Glacier calving during stage 4 released icebergs and growlers, leading to accumulation of boulder-sized glacial dropstones (Figs. 1C–1I; Figs. S3–S5) that generated large impact structures in the sediment and propagated ductile deformation up to 40 cm depth (Fig. S6; Table S1). IRD with evidence of subglacial transport and crushing (Figs. 3A–3G; Figs. S7D–S7E) also accumulated from icebergs during this deglacial stage (Fig. 2A). As deglaciation continued (5 in Fig. 4A), the increasing supply of proglacial sediments led to progradation of a clastic wedge in the lake (Figs. 2A–2B), as also occurred in the Quaternary analog of Baffin Island lakes (fig. 3D of Briner et al., 2007). This clastic wedge (subglacial fan) also contains quartz grains with evidence of subglacial transport (Figs. S7A–S7C).

**Maximum Latitudinal Extent of Glacier Ice during an Enigmatic Cretaceous Climate State**

In the Arctic, there is evidence, including IRD and glendonites, for an active cryosphere during the Hauterivian cold snap (Grasby et al., 2017; Galloway et al., 2019; Vickers et al., 2019; Schneider et al., 2020), but until now, a midlatitude continental record of this global event has remained unrecognized. The Iberian dropstones and IRD reported here provide the first evidence for continental glaciers and glacial-deglacial processes reaching mid-paleolatitudes (42°N–50°N) during the Hauterivian in the Northern Hemisphere (Fig. 4B). The synchronicity of glaciers in the Southern Hemisphere (Alley et al., 2020) with high-altitude plateau permafrost in China (Rodríguez-López et al., 2022) points to a bipolar glaciation associated with the Hauterivian cold snap. Our paleoenvironmental reconstruction (glaciers at 42°N–50°N) matches the maximum latitudinal extent of both the ice cover during the Hauterivian cold snap (Cavalheiro et al., 2021) and the glacier snouts and ice lobes (40°N) during the late Pleistocene LIS (Fig. 4B; Dyke, 2004; Ullman et al., 2015). Coeval with this Hauterivian glaciation, the Early Cretaceous tectonic uplift of Iberia, triggered by the evolution of its plate margins (King et al., 2021), may have lowered glacier equilibrium-line altitudes (ELAs), pushing glacier snouts to reach even lower latitudes. Similar drops in ELAs associated with global glaciations have been reported from the Eocene-Oligocene transition cold snap (EOT-1) in Tibet (Xia et al., 2023) and the late Pleistocene Last Glacial Maximum (LGM) (e.g., dropping ELAs by 980–1000 m in the equatorial Rwenzori Mountains in Uganda and the Democratic Republic of Congo, leaving lateral moraines at ~2.5 km above sea level; Doughty et al., 2023). The Early Cretaceous glaciation of midlatitude continental Iberia was coeval with warm tropical and equatorial seas (e.g., Littler et al., 2011; Price et al., 2020). This synchronicity resembles other temperature discrepancies such as those recorded during the Oligocene (O'Brien et al., 2020), when unexpected warm-temperate conditions in Southern Hemisphere high-latitude sea-surface temperatures (SSTs) coexisted with a large Antarctic ice sheet reaching the margins of the polar continent (Hoem et al., 2022). Reconciliation of translatitudinal paleoclimate proxies will require improved paleoclimate models, with better resolution in marine geochemical records, establishment of more accurate Early Cretaceous paleogeographic and latitudinal reconstructions, and refined dating techniques for both marine and continental records. Collectively, these findings invite reappraisal of the sedimentologic interpretations of Hauterivian–early Barremian records, at least in Iberia (including other Cretaceous dropstones; e.g., Doublet and García, 2004), Eurasia, and North America. Is there further evidence for Early Cretaceous glaciation and periglaciation in northern Eurasia?

## REFERENCES CITED

Alley, N.F., Hore, S.B., and Frakes, L.A., 2020, Glaciations at high-latitude Southern Australia during the Early Cretaceous: Australian Journal of Earth Science, v. 67, p. 1045−1095, https://doi.org/10.1080/08120099.2019.1590457.

Anders E., and Grevesse N., 1989, Abundances of the elements: Meteoritic and solar: Geochimica et Cosmochimica Acta, v. 53, p. 197–214, https://doi.org/10.1016/0016-7037(89)90286-X.

Angrand, P., and Mouthereau, F., 2021, Evolution of the Alpine orogenic belts in the Western Mediterranean region as resolved by the kinematics of the Europe-Africa diffuse plate boundary: Bulletin de la Société Géologique de France, v. 192, 42, https://doi.org/10.1051/bsgf/2021031.

Araújo, R., and Nogueira, A., 2019, Serra Sul diamictite of the Carajás basin (Brazil): A Paleoproterozoic glaciation on the Amazonian craton: Geology, v. 47, p. 1166–1170, https://doi.org/10.1130/G46923.1.

Asti, R., Saspiturry, N., and Angrand, P., 2022, The Mesozoic Iberia-Eurasia diffuse plate boundary: A wide domain of distributed transtensional deformation progressively focusing along the North Pyrenean zone: Earth-Science Reviews, v. 230, https://doi.org/10.1016/j.earscirev.2022.104040.

Briner, J.P., Axford, Y., Forman, S.L., Miller, G.H., and Wolfe, A.P., 2007, Multiple generations of interglacial lake sediment preserved beneath the Laurentide ice sheet: Geology, v. 35, p. 887–890, https://doi.org/10.1130/G23812A.1.

Cavalheiro, L., Wagner, T., Steinig, S., Bottini, C., Dummann, W., Esegbue, O., Gambacorta, G., Giraldo-Gómez, V., Farnsworth, A., Flögel, S., Hofmann, P., Lunt, D.J., Rethemeyer, J., Torricelli, S., and Erba, E., 2021, Impact of global cooling on Early Cretaceous high $p$CO$_2$ world during the Weissert event: Nature Communications, v. 12, 5411, https://doi.org/10.1038/s41467-021-25706-0.

Doublet, S., and García, J.P., 2004, The significance of dropstones in a tropical lacustrine setting, eastern Cameros Basin (Late Jurassic–Early Cretaceous, Spain): Sedimentary Geology, v. 163, p. 293–309, https://doi.org/10.1016/j.sedgeo.2003.07.003.

Doughty, A.M., Kelly, M.A., Russell, J.M., Jackson, M.S., Anderson, B.M., Chipman, J., and Nakileza, B.R., 2023, Last Glacial Maximum reconstructions of Rwenzori Mountain glaciers: Paleoceanography and Paleoclimatology, v. 38, https://doi.org/10.1029/2022PA004527.

Dyke, A.S., 2004, An outline of North American deglaciation with emphasis on central and northern Canada, in Ehlers, J., and Gibbard, P.L., eds., Quaternary Glaciations—Extent and Chronology, Part II: North America: Amsterdam, Netherlands, Elsevier Science and Technology Books, p. 373–424, https://doi.org/10.1016/S1571-0866(04)80209-4.

Galloway, J.M., Vickers, M.L., Price, G.D., Poulton, T., Grasby, S.E., Hadlari, T., Beauchamp, B., and Sulphur, K., 2019, Finding the VOICE: Organic carbon isotope chemostratigraphy of the Late Jurassic–Early Cretaceous of Arctic Canada: Geological Magazine, v. 157, p. 1643–1657, https://doi.org/10.1017/S0016756819001316.

Gao, C., McAndrews, J.H., Wang, X., Menzies, J., Turton, C.L., Wood, B.D., Pei, J., and Kodors, C., 2012, Glaciation of North America in the James Bay Lowland, Canada, 3.5 Ma: Geology, v. 40, p. 975–978, https://doi.org/10.1130/G33092.1.

Grasby, S.E., McCune, G.E., Beauchamp, B., and Galloway, J.M., 2017, Lower Cretaceous cold snaps led to widespread glendonite occurrences in the Sverdrup Basin, Canadian High Arctic: Geological Society of America Bulletin, v. 129, p. 771–787, https://doi.org/10.1130/B31600.1.

Hoem, F.S., Sauermilch, I., Aleksinski, A.K., Huber, M., Peterse, F., Sangiorgi, F., and Bijl, P.K., 2022, Strength and variability of the Oligocene Southern Ocean surface temperature gradient: Communications Earth & Environment, v. 3, 322, https://doi.org/10.1038/s43247-022-00666-5.

Kalińska-Nartiša, E., Lamsters, K., Karušs, J., Krievāns, M., Rečs, A., and Meija, R., 2017, Quartz grain features in modern glacial and proglacial environments: A microscopic study from the Russell Glacier, southwest Greenland: Polish Polar Research, v. 38, p. 265–289, https://doi.org/10.1515/popore-2017-0018.

King, M.T., Welford, J.K., Cadenas, P., and Tugend, J., 2021, Investigating the plate kinematics of the Bay of Biscay using deformable plate tectonic models: Tectonics, v. 40, https://doi.org/10.1029/2020TC006467.

Ladant, J-B., and Donnadieu, Y., 2016, Palaeogeographic regulation of glacial events during the Cretaceous supergreenhouse: Nature Communications, v. 7, https://doi.org/10.1038/ncomms12771.

Le Heron, D.P., 2015, The significance of ice-rafted debris in Sturtian glacial successions: Sedimentary Geology, v. 322, p. 19–33, https://doi.org/10.1016/j.sedgeo.2015.04.001.

Le Heron, D.P., Heninger, M., Baal, C., and Bestmann, M., 2020, Sediment deformation and production beneath soft-bedded Palaeozoic ice sheets: Sedimentary Geology, v. 408, https://doi.org/10.1016/j.sedgeo.2020.105761.

Le Heron, D.P., Busfield, M.E., and Kettler, C., 2021, Ice-rafted dropstones in "postglacial" Cryogenian cap carbonates: Geology, v. 49, p. 263–267, https://doi.org/10.1130/G48208.1.

Le Heron, D.P., Busfield, M.E., Chen, X., Corkeron, M., Davies, B.J., Dietrich, P., Ghienne, J.-F., Kettler, C., Scharfenberg, L., Vandyk, T.M., and Wohlschlägl, R., 2022, New perspectives on glacial geomorphology in Earth's deep time record: Frontiers of Earth Science, v. 10, https://doi.org/10.3389/feart.2022.870359.

Littler, K., Robinson, S.A., Bown, P.R., Nederbragt, A.J., and Pancost, R.D., 2011, High sea-surface temperatures during the Early Cretaceous Epoch: Nature Geoscience, v. 4, p. 169–172, https://doi.org/10.1038/ngeo1081.

Muñoz, A., Angulo, A., Liesa, C.L., Luzón, M.A., Mayayo, M.J., Pérez, A., Soria, A.R., Val, V., and Yuste, A., 2020, Periodicidad climática y datación astrocronológica del Grupo Enciso en la cuenca oriental de Cameros (N de España): Boletín Geológico y Minero, v. 131, p. 243–268, https://doi.org/10.21701/bolgeomin.131.2.003.

Nirrengarten, M., Manatschal, G., Tugend, J., Kusznir, N.J., and Sauter, D., 2017, Nature and origin of the J-magnetic anomaly offshore Iberia-Newfoundland: Implications for plate reconstructions: Terra Nova, v. 29, p. 20–28, https://doi.org/10.1111/ter.12240.

O'Brien, C.L., Huber, M., Thomas, E., Pagani, M., Super, J.R., Elder, L.E., and Hull, P.M., 2020, The enigma of Oligocene climate and global surface temperature evolution: Proceedings of the National Academy of Sciences of the United States of America, v. 117, p. 25,302–25,309, https://doi.org/10.1073/pnas.2003914117.

Price, G.D., Bajnai, D., and Fiebig, J., 2020, Carbonate clumped isotope evidence for latitudinal seawater temperature gradients and the oxygen isotope composition of Early Cretaceous seas: Palaeogeography, Palaeoclimatology, Palaeoecology, v. 552, https://doi.org/10.1016/j.palaeo.2020.109777.

Rodríguez-López, J.P., Liesa, C.L., Pardo, G., Meléndez, N., Soria, A.R., and Skilling, I., 2016, Glacial dropstones in the western Tethys during the late Aptian–early Albian cold snap: Palaeoclimate and palaeogeographic implications for the mid-Cretaceous: Palaeogeography, Palaeoclimatology, Palaeoecology, v. 452, p. 11−27, https://doi.org/10.1016/j.palaeo.2016.04.004.

Rodríguez-López, J.P., Wu, C., Vishnivetskaya, T.A., Murton, J.B., Tang, W., and Ma, C., 2022, Permafrost in the Cretaceous supergreenhouse: Nature Communications, v. 13, 7946, https://doi.org/10.1038/s41467-022-35676-6.

Schneider, S., Kelly, S.R.A., Mutterlose, J., Herrle, J.O., Hülse, P., Jolley, D.W., Schröder-Adams, C.J., and Lopez-Mir, B., 2020, Macrofauna and biostratigraphy of the Rollrock section, northern Ellesmere Island, Canadian Arctic Islands—A comprehensive high latitude archive of the Jurassic-Cretaceous transition: Cretaceous Research, v. 114, https://doi.org/10.1016/j.cretres.2020.104508.

Shrivastava, P.K., Dharwadkar, A., Asthana, R., Roy, S.K., Swain, A.K., and Beg, M.J., 2014, The sediment properties of glacial diamicts from the Jutulsessen area of Gjelsvikfjella, East Antarctica: A reflection of source materials and regional climate: Polar Science, v. 8, p. 264–282, https://doi.org/10.1016/j.polar.2014.03.001.

Stevenard, N., Montero-Serrano, J.-C., Eynaud, F., St-Onge, G., Zaragosi, S., and Copland, L., 2022, Lateglacial and Holocene sedimentary dynamics in northwestern Baffin Bay as recorded in sediment cores from Cape Norton Shaw Inlet (Nunavut, Canada): Boreas, v. 51, p. 532–552, https://doi.org/10.1111/bor.12575.

Ullman, D.J., Carlson, A.E., LeGrande, A.N., Anslow, F.S., Moore, A.K., Caffee, M., Syverson, K.M., and Licciardi, J.M., 2015, Southern Laurentide ice-sheet retreat synchronous with rising boreal summer insolation: Geology, v. 43, p. 23–26, https://doi.org/10.1130/G36179.1.

Vickers, M.L., Price, G.D., Jerrett, R.M., Sutton, P., Watkinson, M.P., and FitzPatrick, M., 2019, The duration and magnitude of Cretaceous cold events: Evidence from the northern high latitudes: Geological Society of America Bulletin, v. 131, p. 1979–1994, https://doi.org/10.1130/B35074.1.

Wu, C.H., and Rodríguez-López, J.P., 2021, Cryospheric processes in Quaternary and Cretaceous hyper-arid oases: Sedimentology, v. 68, p. 755–770, https://doi.org/10.1111/sed.12804.

Xia, G., Wu, C.H., Mansour, A., Jin, X., Yi, H., Li, G., Fan, Q., Shi, Z., Murton, J.B., Pei, J., and Rodríguez-López, J.P., 2023, Eocene–Oligocene glaciation on a high central Tibetan Plateau: Geology, v. 51, p. 559–564, https://doi.org/10.1130/G51104.1.

Printed in the USA